A Nonlinear PIC Algorithm for High Frequency Waves in Magnetized Plasmas Based on Gyrocenter Gauge Kinetic Theory

Jian Liu[1,2], Zhi Yu[3,2,*] and Hong Qin[1,4]

[1] *Department of Modern Physics and Collaborative Innovation Center for Advanced Fusion Energy and Plasma Sciences, University of Science and Technology of China, Hefei, Anhui 230026, China.*
[2] *Key Laboratory of Geospace Environment, University of Science and Technology of China, Chinese Academy of Sciences, Hefei, Anhui 230026, China.*
[3] *Theory and Simulation Division, Institute of Plasma Physics, Chinese Academy of Sciences, Hefei, Anhui 230031, China.*
[4] *Plasma Physics Laboratory, Princeton University, Princeton, New Jersey 08543, USA.*

Abstract. Numerical methods based on gyrocenter gauge kinetic theory are suitable for first principle simulations of high frequency waves in magnetized plasmas. The δf gyrocenter gauge PIC simulation for linear rf wave has been previously realized. In this paper we further develop a full-f nonlinear PIC algorithm appropriate for the nonlinear physics of high frequency waves in magnetized plasmas. Numerical cases of linear rf waves are calculated as a benchmark for the nonlinear GyroGauge code, meanwhile nonlinear rf-wave phenomena are studied. The technique and advantage of the reduction of the numerical noise in this full-f gyrocenter gauge PIC algorithm are also discussed.

1 Introduction

Radio frequency (rf) waves have been theoretically proposed and experimentally proved an effective method for plasma heating and current drive in magnetic confinement fu-

Corresponding author. Email addresses: `jliuphy@ustc.edu.cn` (J. Liu), `yuzhi@ipp.ac.cn` (Z. Yu), `hongqin@ustc.edu.cn` (H. Qin)

sion (MFC) research [1–4]. Recent research shows strong evidences that toroidal plasma rotations can be induced by rf waves launching in tokamaks [5–7]. These facts reflect that rf waves launching is important to improve confinement and to maintain H-mode runs of tokamaks. On the other hand, our understanding on the physics of rf waves in magnetized plasmas is still limited. The multi-scale and nonlinear properties of rf physics in magnetized plasmas bring challenges to theoretical analysis. First principle simulations build a bridge between theories and experiments for rf wave research. To numerically study rf waves, an efficient algorithm is thus required. A δf particle-in-cell (PIC) algorithm based on gyrocenter gauge kinetic theory has been successfully applied to linear rf wave simulation [8]. In this paper, we further develop a full-f gyrocenter gauge PIC algorithm which is appropriate for the description of nonlinear rf wave physics.

Because the frequencies of rf waves are high enough, the high-frequency responses of charged particles in magnetized plasmas, as well as the changes of their gyro-orbits, have to be taken into account. This indicates that the length of time step in rf wave simulations should be extremely small compared with the time scale of the problem, which brings along heavy computational burdens. Traditional gyrokinetic theory improves numerical efficiency through averaging out the fast gyromotion of charged particles and only sustain the slow gyrocenter dynamics. Though traditional gyrokinetics is a powerful tool for low frequency physics, it cannot be applied to rf-wave simulation directly because the fast responses of charged particles are erased by gyro-average.

Gyrocenter gauge kinetic theory is a special version of the generalized kinetic theory, which deal with the Vlasov-Maxwell system in a geometric view [9–11]. Gyrocenter gauge kinetic theory is aimed to solve the multi-time-scale problems, such as the high frequency waves in magnetized plasmas. In the theory, fast gyromotion of charged particles is decoupled from slow gyrocenter dynamics instead of being removed by gyro-average. Then particle dynamics with different time-scales can be advanced separately in different time steps. When decoupling dynamics with different time-scales, the key step is to find a proper symmetry, which is the gyro-symmetry in the case of charged particles in magnetized plasmas. However, the existence of high frequency electromagnetic perturbations breaks the original gyro-symmetry. gyrocenter gauge kinetic theory resolves it through a second gyrocenter coordinate transform using Lie perturbation method.

Traditional gyrokinetics consists of two pivotal steps, gyrocenter coordinate transform and gyrophase average. Gyrocenter gauge kinetic theory shares the first step with traditional gyrokinetics. In this first gyrocenter coordinate transform, particle coordinate $(\mathbf{x},\mathbf{v})$ is transformed to unperturbed gyrocenter coordinate $\tilde{\mathbf{Z}} = (\tilde{\mathbf{X}},\tilde{u},\tilde{\mu},\tilde{\theta})$, where $\mathbf{x}$ is particle position coordinate, $\mathbf{v}$ is particle velocity coordinate, $\tilde{\mathbf{X}}$ is gyrocenter position coordinate, $\tilde{u}$ is parallel velocity, $\tilde{\mu}$ is magnetic moment, and $\tilde{\theta}$ is gyrophase. Yet in gyrocenter gauge kinetic theory, a second gyrocenter coordinate transform is needed to transform the unperturbed gyrocenter coordinate $\tilde{\mathbf{Z}}$ to the perturbed gyrocenter coordinate $\mathbf{Z} = (\mathbf{X},u,\mu,\theta)$. The second gyrocenter coordinate transform employs Lie coordinate perturbation method and thus requires assumption that high frequency perturbations are not strong enough to violently break the original gyro-symmetry. This assumption

means that the differences between two sets of gyrocenter coordinates are higher order small values, which can be guaranteed if the magnitude of high frequency perturbation is small and magnetic confinement still holds. Finally, the distribution function in particle coordinate $f(\mathbf{x},\mathbf{v})$ is replaced by two distribution functions, the gyrocenter distribution function $F(\mathbf{X},u,\mu)$ and a gauge function $S(\mathbf{X},u,\mu,\theta)$. The gyrocenter distribution function F, which describe slow dynamics of gyrocenters, does not depend on gyrophase and advances at large time step. Gauge function S contains dynamics of fast time-scale and can be sampled intensively through a structure called Kruskal ring [12]. These techniques enable algorithms based on gyrocenter gauge kinetic theory to take sample in a more efficient way compared with full kinetic 6D simulations [13, 14].

In PIC method, fields are sampled on Euler grids fixed in configuration space, therefore distribution of electric current density in particle coordinate are required. Since the evolution of charged particles are advanced in gyrocenter coordinate, the calculation of electric current density involves pullback transformation. In previous linear algorithm [8], first-order term of perturbation current density is obtained directly by analytic integration and then fed into Maxwell equations. This method is a kind of δf method because zero-order current density, the equilibrium quantity, does not appear. It can reduce numerical noises evidently. However, nonlinear phenomena require more higher-order terms, which are too complex to calculate. The nonlinear algorithm abandons this series expansion technique. Current density, which include all terms in the series expansion, is given directly by pullback transformation, see Eqs. (2.29)-(2.31). In Section 2, we construct the nonlinear algorithm based on gyrocenter gauge kinetic theory for high frequency waves in magnetized plasmas. Then in Section 3, some numerical results using this method are presented, including both linear and nonlinear cases. Linear cases are used as benchmarks to show the correctness of this algorithm, meanwhile nonlinear cases, such as frequency doubling phenomena, are simulated. In Section 4, we give a brief discussion and the future plan.

2   Nonlinear algorithm based on gyrocenter gauge kinetic theory

In this section, we construct the nonlinear algorithm for high frequency waves in magnetized plasmas based on gyrocenter gauge kinetic theory. We start from the Poincaré-Cartan-Einstein one-form γ in the particle coordinate

$$\gamma(\mathbf{x},\mathbf{v}) = (q\mathbf{A} + m\mathbf{v})\cdot \mathrm{d}\mathbf{x} - \left(q\phi + \frac{1}{2}mv^2\right)\mathrm{d}t, \qquad (2.1)$$

where $\mathbf{A}$ denotes the potential vector, ϕ denotes the potential scalar, q is the electric charge, and m is the mass of the charged particle. This one-form can be transformed to the unperturbed gyrocenter coordinate $\tilde{\mathbf{Z}} = (\tilde{\mathbf{X}}, \tilde{u}, \tilde{\mu}, \tilde{\theta})$ through the first gyrocenter co-

ordinate transform. The transform relation satisfies

$$\mathbf{x} = \tilde{\mathbf{X}} + \boldsymbol{\rho} = \tilde{\mathbf{X}} + \frac{m\tilde{w}}{qB_0}\mathbf{a}, \tag{2.2}$$

$$\mathbf{v} = \tilde{u}\mathbf{b} + \tilde{w}\mathbf{c}, \tag{2.3}$$

where B_0 denotes the background magnetic field at the position of the gyrocenter, $\mathbf{b}$ is a unit vector along $\mathbf{B}_0$, $\mathbf{a}$ is a unit vector parallel to the gyro-radius $\boldsymbol{\rho}$, and $\mathbf{c}$ is a unit vector along the perpendicular component of velocity.

In the nonuniform background magnetic field, a set of local frame should be chosen. We choose two unit vectors, $\mathbf{e}_1$ and $\mathbf{e}_2$, perpendicular to $\mathbf{b}$ satisfying $\mathbf{e}_1 \times \mathbf{e}_2 = \mathbf{b}$, that is $\mathbf{e}_1$, $\mathbf{e}_2$ and $\mathbf{b}$ constitute a local right-handed orthogonal frame. In this local frame, unit vectors $\mathbf{a}$ and $\mathbf{c}$ are expressed as

$$\mathbf{a}(\tilde{\theta}) = \cos\tilde{\theta}\mathbf{e}_1 + \sin\tilde{\theta}\mathbf{e}_2, \tag{2.4a}$$

$$\mathbf{c}(\tilde{\theta}) = \sin\tilde{\theta}\mathbf{e}_1 - \cos\tilde{\theta}\mathbf{e}_2. \tag{2.4b}$$

This relation can be in turn taken as the definition of the gyrophase. We can also write down the following relations

$$\mathbf{a} \times \mathbf{b} = \mathbf{c}, \quad \mathbf{b} = \frac{\mathbf{B}_0}{B_0}, \tag{2.5a}$$

$$\frac{\partial \mathbf{a}}{\partial \tilde{\theta}} = -\mathbf{c}, \quad \frac{\partial \mathbf{c}}{\partial \tilde{\theta}} = \mathbf{a}. \tag{2.5b}$$

Moreover, the magnetic moment and the gyro-radius are respectively defined as

$$\tilde{\mu} = \frac{m\tilde{w}^2}{2B_0}, \quad \boldsymbol{\rho} = \frac{1}{q}\sqrt{\frac{2m\tilde{\mu}}{B_0}}\mathbf{a}. \tag{2.6}$$

Each field quantity can be expressed as the summation of a slow varying background part and a fast varying perturbation part. Given there is no background electric field, we can write these field quantities as

$$\mathbf{B} = \mathbf{B}_0 + \mathbf{B}_1, \quad \mathbf{E} = \mathbf{E}_1, \tag{2.7a}$$

$$\mathbf{A} = \mathbf{A}_0 + \mathbf{A}_1, \quad \phi = \phi_1, \tag{2.7b}$$

$$\mathbf{E} = -\nabla\phi - \frac{\partial \mathbf{A}}{\partial t}, \quad \mathbf{B} = \nabla \times \mathbf{A}. \tag{2.7c}$$

According to Eqs. (2.2)-(2.7), the one-form in unperturbed gyrocenter coordinate $\tilde{\mathbf{Z}}$ takes the form

$$\tilde{\gamma}(\tilde{\mathbf{Z}}) = q\mathbf{A}_0 \cdot d\tilde{\mathbf{X}} + m\tilde{u}\mathbf{b} \cdot d\tilde{\mathbf{X}} - \frac{m\tilde{\mu}}{q}d\tilde{\theta} - q\phi_1(\mathbf{x},t)dt - \left(\frac{1}{2}m\tilde{u}^2 + \tilde{\mu}B_0\right)dt$$

$$+ \mathbf{A}_1(\mathbf{x},t) \cdot \left(qd\tilde{\mathbf{X}} + \sqrt{\frac{m}{2\tilde{\mu}B_0}}\mathbf{a}d\tilde{\mu} - \sqrt{\frac{2m\tilde{\mu}}{B_0}}\mathbf{c}d\tilde{\theta}\right). \tag{2.8}$$

We further assume that the background magnetic field changes very slowly with space just for simplicity. This assumption neglects the effects caused by the nonuniform of the background field, such as the gyrocenter drift motion, but has no impact on high frequency physics. The one-form γ determines the behaviors of charged particles in the electromagnetic fields. To decouple the dynamics with different time-scales, we could divide the one-form into two parts. One depends only on the background fields $\tilde{\gamma}_0$ and the other depends on perturbation fields $\tilde{\gamma}_1$. Their explicit expressions are

$$\tilde{\gamma}_0(\tilde{\mathbf{Z}}) = (q\mathbf{A}_0 + m\tilde{u}\mathbf{b}) \cdot \mathrm{d}\tilde{\mathbf{X}} - \frac{m\tilde{\mu}}{q}\mathrm{d}\tilde{\theta} - \left(\frac{1}{2}m\tilde{u}^2 + \tilde{\mu}B_0\right)\mathrm{d}t, \tag{2.9}$$

and

$$\tilde{\gamma}_1(\tilde{\mathbf{Z}}) = \mathbf{A}_1(\mathbf{x},t) \cdot \left(q\mathrm{d}\tilde{\mathbf{X}} + \sqrt{\frac{m}{2\tilde{\mu}B_0}}\mathbf{a}\mathrm{d}\tilde{\mu} - \sqrt{\frac{2m\tilde{\mu}}{B_0}}\mathbf{c}\mathrm{d}\tilde{\theta}\right) - q\phi_1(\mathbf{x},t)\mathrm{d}t. \tag{2.10}$$

In Eq. (2.10), $\mathbf{A}_1$, ϕ_1, $\mathbf{a}$ and $\mathbf{c}$ are all quantities with the fast time scale. Note that this partition of one-form is in some extent arbitrary.

Now, Lie perturbation method can be used to the second gyrocenter coordinate transform, which transforms unperturbed gyrocenter coordinate $\tilde{\mathbf{Z}}$ to perturbed gyrocenter coordinate $\mathbf{Z}$. The transform relation is

$$\mathbf{Z} = \tilde{\mathbf{Z}} + \mathbf{G}. \tag{2.11}$$

Given the magnitudes of the perturbation fields are much smaller than that of the background fields, $\mathbf{G}$ is much smaller than $\mathbf{Z}$. Then we have

$$\gamma(\mathbf{Z}) = \tilde{\gamma}(\tilde{\mathbf{Z}}) = \tilde{\gamma}(\mathbf{Z} - \mathbf{G}) = \tilde{\gamma}(\mathbf{Z}) - i_\mathbf{G}\mathrm{d}\tilde{\gamma}(\mathbf{Z}). \tag{2.12}$$

In perturbed gyrocenter coordinate, γ_1 takes the form

$$\gamma_1(\mathbf{Z}) = \tilde{\gamma}_1(\mathbf{Z}) - i_\mathbf{G}\mathrm{d}\tilde{\gamma}_0(\mathbf{Z}) + \mathrm{d}S(\mathbf{Z}), \tag{2.13}$$

where S is called gauge function, satisfying

$$\mathrm{d}S(\mathbf{Z}) = \tilde{\gamma}_0(\mathbf{Z}) - \gamma_0(\mathbf{Z}). \tag{2.14}$$

We have to appeal to gyro-symmetry now to accomplish the decouple of different time scales. The gyro-symmetry demand the relation $\partial\gamma_1/\partial\theta = 0$ holds, that is γ_1 is independent of gyrophase θ. Under the limit of this prerequisite, there is still a freedom left for the choice of $S(\mathbf{Z})$. Different choices of S brings different expressions for γ_1. Essentially, the choice of S is a kind of gauge choice. That's why S is called gauge function and why the theory is named gyrocenter gauge kinetic theory. Different gauge choices only influence the complexity of computation, but doesn't change the real physics.

The second term in Eq. (2.13) can be proved as

$$i_{\mathbf{G}}\mathrm{d}\tilde{\gamma}_0(\mathbf{Z}) = (q\mathbf{B}_0 \times \mathbf{G}_{\mathbf{X}} + mG_u\mathbf{b}) \cdot \mathrm{d}X + (muG_t - m\mathbf{b} \cdot \mathbf{G}_{\mathbf{x}})\,du$$
$$+ \left(\frac{m}{q}G_\theta + B_0 G_t\right)\mathrm{d}\mu - \frac{m}{q}G_\mu\mathrm{d}\theta - (muG_u + B_0 G_\mu)\,\mathrm{d}t, \tag{2.15}$$

where $G_t = 0$ because there is no transform for the time coordinate. Then the expression of γ_1 is

$$\gamma_1(\mathbf{Z}) = (q\mathbf{A}_1(\mathbf{x},t) - q\mathbf{B}_0 \times \mathbf{G}_{\mathbf{X}} - mG_u\mathbf{b} + \nabla S) \cdot \mathrm{d}X + \left(m\mathbf{b} \cdot \mathbf{G}_{\mathbf{x}} + \frac{\partial S}{\partial u}\right)du$$

$$+ \left(\sqrt{\frac{m}{2\mu B_0}}\mathbf{A}_1(\mathbf{x},t) \cdot \mathbf{a} - \frac{m}{q}G_\theta + \frac{\partial S}{\partial \mu}\right)\mathrm{d}\mu + \left(-\sqrt{\frac{2m\mu}{B_0}}\mathbf{A}_1(\mathbf{x},t) \cdot \mathbf{c} + \frac{m}{q}G_\mu + \frac{\partial S}{\partial \theta}\right)\mathrm{d}\theta$$

$$+ \left(-q\phi_1(\mathbf{x},t) + muG_u + B_0 G_\mu + \frac{\partial S}{\partial t}\right)\mathrm{d}t. \tag{2.16}$$

We choose a gauge S which simply makes

$$\gamma_1(\mathbf{Z}) = 0 \tag{2.17}$$

hold. Then the evolution equation, which S obeys, is

$$\frac{\partial S}{\partial t} + u\mathbf{b} \cdot \nabla S - \frac{qB_0}{m}\frac{\partial S}{\partial \theta} = q\phi_1(\mathbf{x},t) - qu\mathbf{b} \cdot \mathbf{A}_1(\mathbf{x},t) - q\sqrt{\frac{2\mu B_0}{m}}\mathbf{A}_1(\mathbf{x},t) \cdot \mathbf{c}. \tag{2.18}$$

At the same time, we can get the evolution equations for $\mathbf{G}$ as

$$\mathbf{G}_{\mathbf{X}} = -\frac{1}{m}\frac{\partial S}{\partial u}\mathbf{b} - \frac{1}{B_0}\mathbf{b} \times \mathbf{A}_1(\mathbf{x},t) - \frac{1}{qB_0}\mathbf{b} \times \nabla S, \tag{2.19a}$$

$$G_\mu = \frac{q}{m}\left(\sqrt{\frac{2m\mu}{B_0}}\mathbf{A}_1(\mathbf{x},t) \cdot \mathbf{c} - \frac{\partial S}{\partial \theta}\right), \tag{2.19b}$$

$$G_u = \frac{q}{m}\mathbf{b} \cdot \mathbf{A}_1(\mathbf{x},t) + \frac{1}{m}\mathbf{b} \cdot \nabla S, \tag{2.19c}$$

$$G_\theta = \frac{q}{m}\left(\sqrt{\frac{m}{2\mu B_0}}\mathbf{A}_1(\mathbf{x},t) \cdot \mathbf{a} + \frac{\partial S}{\partial \mu}\right). \tag{2.19d}$$

According to Hamilton's principle, the dynamics of the charged particle follow the rule

$$i_\tau \mathrm{d}\gamma = 0. \tag{2.20}$$

Then we have

$$\tau_X = u\tau_t\mathbf{b}, \tag{2.21a}$$
$$\tau_u = 0, \tag{2.21b}$$
$$\tau_\mu = 0, \tag{2.21c}$$
$$\tau_\theta = -\frac{qB_0}{m}\tau_t, \tag{2.21d}$$

and the equations of motion for the gyrocenters as

$$\frac{d\mathbf{X}}{dt} = \frac{\tau_X}{\tau_t} = u\mathbf{b}, \tag{2.22a}$$

$$\frac{du}{dt} = \frac{\tau_u}{\tau_t} = 0, \tag{2.22b}$$

$$\frac{d\mu}{dt} = \frac{\tau_\mu}{\tau_t} = 0, \tag{2.22c}$$

$$\frac{d\theta}{dt} = \frac{\tau_\theta}{\tau_t} = -\frac{qB_0}{m}. \tag{2.22d}$$

The distribution function for gyrocenters F thus satisfies

$$\frac{\partial F}{\partial t} + u\mathbf{b}\cdot\nabla_{\mathbf{X}}F - \frac{qB_0}{m}\frac{\partial F}{\partial\theta} = 0, \tag{2.23}$$

and the gauge function S satisfies

$$\frac{dS}{dt} = q\phi_1(\mathbf{x},t) - qu\mathbf{b}\cdot\mathbf{A}_1(\mathbf{x},t) - q\sqrt{\frac{2\mu B_0}{m}}\mathbf{A}_1(\mathbf{x},t)\cdot\mathbf{c}. \tag{2.24}$$

According to Eq. (2.19), the calculation of G_μ and G_θ requires the value of $\partial S/\partial\theta$ and $\partial S/\partial\mu$. They can be obtained from the partial derivative of Eq. (2.24) as

$$\frac{d}{dt}\frac{\partial S}{\partial\mu} = \frac{\partial}{\partial\mu}\frac{dS}{dt} = \sqrt{\frac{m}{2\mu B_0}}\mathbf{a}\cdot\nabla\phi_1(\mathbf{x},t) - u\sqrt{\frac{m}{2\mu B_0}}\mathbf{a}\cdot\nabla(\mathbf{b}\cdot\mathbf{A}_1(\mathbf{x},t))$$

$$- \mathbf{a}\cdot\nabla(\mathbf{A}_1(\mathbf{x},t)\cdot\mathbf{c}) - q\sqrt{\frac{B_0}{2m\mu}}\mathbf{A}_1(\mathbf{x},t)\cdot\mathbf{c}, \tag{2.25}$$

and

$$\frac{d}{dt}\frac{\partial S}{\partial\theta} = \frac{\partial}{\partial\theta}\frac{dS}{dt} = -\sqrt{\frac{2m\mu}{B_0}}\mathbf{c}\cdot\nabla\phi_1(\mathbf{x},t) + u\sqrt{\frac{2m\mu}{B_0}}\mathbf{c}\cdot\nabla(\mathbf{b}\cdot\mathbf{A}_1(\mathbf{x},t))$$

$$+ 2\mu\mathbf{c}\cdot\nabla(\mathbf{A}_1(\mathbf{x},t)\cdot\mathbf{c}) - q\sqrt{\frac{2\mu B_0}{m}}\mathbf{A}\cdot\mathbf{a}. \tag{2.26}$$

At the moment, we successfully obtain the decoupled gyrocenter gauge kinetic equations. The evolution of the gyrocenter distribution function F depends only on the background magnetic field. All the fast kinetic effects are included in the evolution of the gauge function S. The next task is to calculate the correct response current density according to the particle distribution in perturbed gyrocenter coordinate.

In previous linear gyrocenter gauge kinetic algorithm [8], the first-order term of current density are analytically calculated using pullback transformation and series expansion as

$$\hat{\mathbf{J}}_\perp(\mathbf{r}) = -\frac{2B_0}{v_T^2}\sum_{i,j}^{n,m}\kappa_i\Delta(\mathbf{X}_i+\boldsymbol{\rho}_{i,j}-\mathbf{r})\mathbf{V}_{i,j}^\perp\left[(\mathbf{V}_{i,j}^\perp+u\mathbf{b})\cdot\mathbf{A}_1(\mathbf{X}_i+\boldsymbol{\rho}_{i,j})+B_0\partial_\theta S_{i,j}\right], \tag{2.27}$$

where $\hat{\mathbf{J}}_\perp(\mathbf{r})$ denotes current density perpendicular to the background magnetic field, v_T is thermal velocity, κ_i denotes the weight of the ith gyrocenter, $\mathbf{V}_{i,j}^\perp$ and $\boldsymbol{\rho}_{i,j}$ are the perpendicular velocity and the gyro-radius of the jth sampling point on the Kruskal ring carried by the ith gyrocenter respectively, $\mathbf{X}_i$ is the spatial position of the ith gyrocenter. This method is a type of δf method, which doesn't count in the contribution from unperturbed background electric current density as well as the higher order terms. It has the advantage of low numerical noises, but is inconvenient for nonlinear simulation. On the one hand, nonlinear phenomena involves the higher order terms in the series expansion of current density. These higher order terms are more difficulty to handle for analytic deduction and too resource consuming for numerical computation. On the other hand, it is impossible to calculate all the expansion terms, which means strong nonlinear phenomena cannot be fully described by this means. Further more, in the future large-scale integrated rf wave simulations the equilibrium quantities may also change with time, which can not be dealt with by the linear expansion algorithm. So we need a more effective way to calculate the current density for nonlinear rf wave physics.

According to the twice gyrocenter coordinate transforms and corresponding pullback transformation, it is feasible to calculate the current density in particle coordinate directly from its definition as

$$\mathbf{j}(\mathbf{r}) = -e \int f(\mathbf{r},\mathbf{v})\mathbf{v} \, \mathrm{d}^3\mathbf{v}. \tag{2.28}$$

Its discrete version which can be used in numerical simulation is

$$\mathbf{j}(\mathbf{r}) = -e \sum_{i,j}^{n,m} \kappa_i \Delta(\mathbf{x}_{i,j}-\mathbf{r})\mathbf{v}_{i,j}, \tag{2.29}$$

where $\mathbf{x}$ and $\mathbf{v}$ denote the position and velocity of charged particles in particle coordinate. They can be achieved from the pullback transform from perturbed gyrocenter coordinate as

$$\mathbf{x} = \mathbf{X} - \mathbf{G_X} + \frac{m}{qB_0}\sqrt{\frac{2B_0(\mu-G_\mu)}{m}}\left[\cos(\theta-G_\theta)\mathbf{e}_x + \sin(\theta-G_\theta)\mathbf{e}_y\right], \tag{2.30}$$

$$\mathbf{v} = \sqrt{\frac{2B_0(\mu-G_\mu)}{m}}\left[\sin(\theta-G_\theta)\mathbf{e}_x - \cos(\theta-G_\theta)\mathbf{e}_y\right] + (u-G_u)\mathbf{e}_z. \tag{2.31}$$

The current density obtained from this method contains the contribution from the distribution of the background plasmas. For example the polarization current density caused by the density gradient of the background plasmas can be achieved directly by this method.

The coordinate transform and corresponding pull-back transform are both exact, so all the nonlinear effects of the gyrocenter system are kept. The approximation only exists in Eq. (2.12), where the higher order terms of the 1-form are dropped. The equations for X

and S are based on this expansion, which means that the gyrocenter system is not exactly equivalent to the original particle system. The Lagrangian densities of the gyrocenter system and the original particle system differ by the higher order terms. In this sense, some higher- order nonlinear terms of the original particle system are still missing in the gyrocenter gauge algorithm.

To calculate the nonlinear physics of the original particle system more accurately, the idea to keep the second-order term in Eq. (2.12) has been proposed to decrease the differences between the two systems. However, this treatment brings computational complexities evidently. If **G** is large enough, more higher-order terms should be kept to make sure that the difference between the gyrocenter system and the original particle system is small, and this scheme is impractical. A more efficient method is used in the gyrocenter gauge algorithm to solve this problem. The initial value of **G** is zero, but the value of **G** could grow larger and larger by accumulation. When the value of **G** goes higher than a relative threshold ϵ, this time should be taken as a new starting point for the transform. The coordinate transform $\mathbf{Z} \rightarrow \tilde{\mathbf{Z}}$ is restarted at this time step, and **G** is reset to zero again. Then another gyrocenter system, which is a better approximation to the original particle system, is found at this time step. The difference between the Lagrangian density of the gyrocenter system and that of the original particle system is always smaller than ϵ. The accuracy of the particle system's nonlinear phenomena is thus determined by the value of the threshold ϵ. Because at each time step the particle coordinates have been calculated to give the current, it is convenient to carry out the new coordinate transform without any extra computation cost.

Once the correct current density is obtained, it can be used to compute the field quantities on the Euler grids through Ampère's circuital law

$$\nabla \times \mathbf{B} = \mu_0 \epsilon_0 \frac{\partial \mathbf{E}}{\partial t} + \mu_0 \mathbf{j}. \tag{2.32}$$

Taken the Weyl gauge, also known as the temporal gauge, $\phi = 0$ to the electromagnetic potential, we have

$$\mathbf{E} = -\frac{\partial \mathbf{A}}{\partial t}, \tag{2.33}$$

$$\mathbf{B} = \nabla \times \mathbf{A}, \tag{2.34}$$

and the equation for the potential vector

$$\nabla \times \nabla \times \mathbf{A} + \frac{1}{c^2} \frac{\partial^2 \mathbf{A}}{\partial t^2} = \mu_0 \mathbf{j}. \tag{2.35}$$

The current density **j** on the right-hand side of the equation reflects the responses from the plasmas to the evolution of the electromagnetic fields. Then with the equations of the particle dynamics, the method to calculate the current density, and the equation for the field, the whole flow chart of the algorithm is completed, see Fig. 1. We will practise this algorithm with some rf wave problems in magnetized plasmas in Section 3.
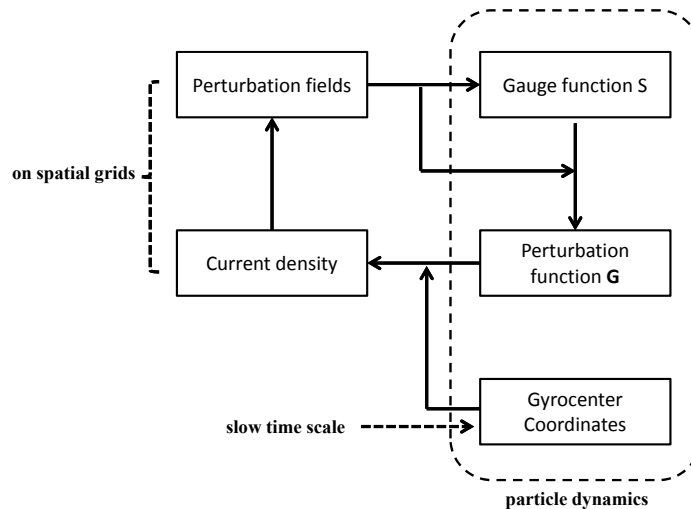
Figure 1: Flow chart of simulation.Within each loop of time advance, particles' dynamics, including gyrocenter coordinates and gauge function, is calculated from fields on grids and then gives the current density on grids. The current density in turn gives the fields. Gyrocenter coordinates advance at large time step because its slow time-scale dynamics. So the computation consumption on gyrocenter coordinates can be neglected.

3   Numerical cases

Based on the algorithm introduced in Section 2, the rf waves in magnetized plasmas can be studied through the first-principle gyrocenter gauge kinetic simulation. In this section, we carry out some numerical simulations of high frequency waves in magnetized plasmas to verify the correctness and effectiveness of this method. In these cases, we focus on the waves with frequencies around the gyro-frequency of the electrons. Then for simplicity, the ions can be taken as the continuous positively-charged background for the electrons because the response from the ions to the waves with such high frequencies can be neglected.

At first, the linear physics of the rf waves is reproduced as benchmarks to the gyrocenter gauge algorithm. The simulation code used here is in principle a nonlinear one, which means the simulation results contain all the nonlinear physics of the particle-field system, similar to the experimental results in the real lab. However, the linear phenomena can still be recovered from this nonlinear code by decreasing the amplitudes of the electromagnetic perturbations to a very low level. The nonlinear effects are thus suppressed.

The magnetized plasma is set to be uniformly distributed in the configuration space with the periodic boundary conditions in the **x**, **y**, and **z** directions. The external background magnetic field $\mathbf{B}_0$ is along the **z** direction. The electromagnetic perturbations with small amplitude are initialized in the spacial region. The evolution of the electromagnetic perturbations and the motion of electrons are computed following the nonlinear gyrocenter gauge kinetic PIC method. To reproduce linear results, the amplitude of the

perturbations is set to be small enough to make sure that the change of the magnetic moment μ caused by the electromagnetic waves is much smaller than the value of μ itself. Meanwhile, we set the number density of the electrons to be $n_e = 10^{20}/m^3$ and the background magnetic field to be $B_0 = 5T$. In each direction of the configuration space region 400 sampling grids are taken, and the distance between two adjacent grids is $0.25mm$. Ten sampling points for the electrons are taken on each Kruskal ring to meet the desired precision. If adjusting the thermal velocity of the electrons to let their gyro-radii be much smaller than the wavelength, that is $k \ll 1/\rho_e$, we obtain the dispersion relation of X waves, see Fig. 2, and O waves, see Fig. 3, in cold plasmas. The same dispersion relations can also be achieved by rigorous analytic calculation [15]. According to the analytic results, the dispersion relation of X waves in cold plasmas satisfies

$$c^2 k^2 = \omega^2 - \omega_{pe}^2 \frac{\omega^2 - \omega_{pe}^2}{\omega^2 - \omega_{UH}^2}, \tag{3.1}$$

where ω_{pe} is the electron plasma frequency, ω_{UH} is the upper-hybrid resonant frequency, satisfying

$$\omega_{UH}^2 = \Omega_e^2 + \omega_{pe}^2, \tag{3.2}$$

and Ω_e is the electron gyro-frequency. And moreover, the dispersion relation of O waves in cold plasmas satisfies

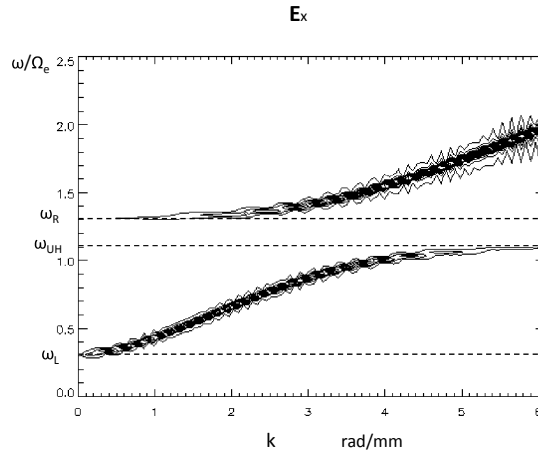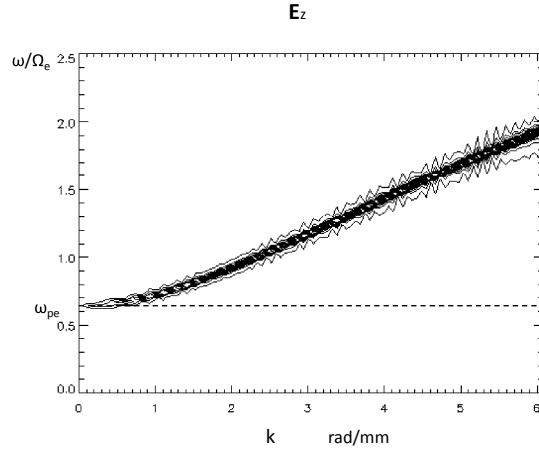$$c^2 k^2 = \omega^2 - \omega_{pe}^2. \tag{3.3}$$

Figure 2: Contour plot of the x component of electric perturbation E_x in spectrum space. The abscissa denotes wave vector in **y** direction in unit of rad/mm. The ordinate denotes frequency ω of perturbed field E_x in the unit of electron gyro-frequency Ω_e. This plot depicts the dispersion relation of X waves propagating perpendicular to the background field. The three horizonal dotted lines mark the value of ω_R, ω_{UH} and ω_L respectively.

E_z

Figure 3: Contour plot of the y component of electric perturbation E_y in spectrum space. The abscissa denotes wave vector in **y** direction in unit of rad/mm. The ordinate denotes frequency ω of perturbed field E_y in the unit of electron gyro-frequency Ω_e. This plot depicts the dispersion relation of O waves propagating perpendicular to the background field. The horizonal dotted line marks the value of ω_{pe}.

It's obvious that for X waves there are two cutoff frequencies,

$$\omega_{R,L} = \sqrt{\left(\frac{\Omega_e}{2}\right)^2 + \omega_{pe}^2} \pm \frac{\Omega_e}{2}, \qquad (3.4)$$

and a resonance frequency ω_{UH}, while for O waves there exists only one cutoff frequency ω_{pe}. According to the parameter setup in this case, the values of these characteristic frequencies are $\omega_{pe} = 0.64\Omega_e$, $\omega_R = 1.31\Omega_e$, $\omega_L = 0.31\Omega_e$, and $\omega_{UH} = 1.19\Omega_e$ respectively. By comparison, it turns out that the first-principle simulation results fits the analytical ones perfectly.

When the gyro-radii are set to be about the same size with wavelength, that is $k\rho_e \gtrsim 1$, by adjusting the electron temperature, the finite Larmor radius effect begins to appear. The dispersion relations of perpendicularly propagating waves are different from those in the long-wavelength case. The simulation results in Fig. 4 exhibit the dispersion relations of perpendicularly propagating waves with short wavelengths. With the increase of the wavelength k, the component of the electric field perturbation in the **x** direction, which is perpendicular to the wave propagation direction, disappears and the wave develops into the electron Bernstein waves. An interesting phenomenon is that the slow X wave may connect to different branches of electron Bernstein wave in the dispersion relation diagram, with the change of ω_{UH}/Ω_e. For different plasma parameters, the mode conversion of the slow X wave to the electron Bernstein wave is different. It is also can be observed that the lower branches of the electron Bernstein wave, the branches near the resonance frequency, have stronger amplitudes.

The second case represents the process of a rf wave launching into a spatially nonuniform plasma from the low-density side. The density profile of the magnetized plasma
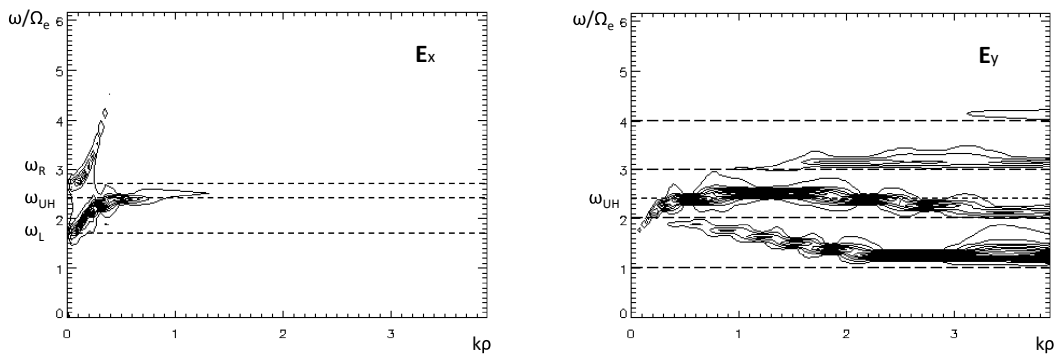
Figure 4: Dispersion relations for perpendicularly propagating waves in magnetized plasmas for short wavelength. The left one is the contour plot of E_x in spectrum space. The right one is the contour plot of E_y in spectrum space. The abscissa denotes the value of $k\rho_e$, the ordinate denotes the value of ω/Ω_e. Several horizonal dotted lines marked the value of ω_L, ω_R, ω_{UH}, ω_{UH}, and harmonic resonance frequencies $\omega_n = n\Omega_e$. In this case, plasma parameters are set to fit $\omega_{pe} = 2.13\Omega_e$.

in the wave propagation direction, **y** direction, is depicted by Fig. 5. The uniform background magnetic field is still along the **z** direction with the magnitude $B_0 = 4T$. The rf wave is launched into the plasma from left, with the frequency $\omega_{in} = 1.5\Omega_e$. The injection wave is set to be linearly polarized in the vacuum. Its original polarization direction is along the **x** direction. In Fig. 5, the position of the plasma boundary and the places where the wave frequency equals the local right-handed cutoff frequency, $\omega_{in} = \omega_R$, and the local upper-hybrid resonance frequency, $\omega_{in} = \omega_{UH}$, are indicated by vertical dotted lines. The right-side boundary condition of this region is set to be the absorption layer condition, avoiding wave reflection from this boundary.
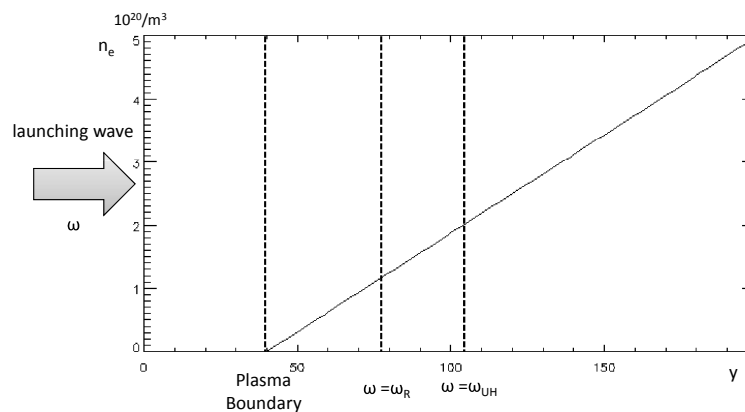

Figure 5: Profile of electron number density n_e along **y**. The abscissa denotes the grid number in **y** direction. The ordinate denotes electron number density. A rf with frequency $\omega = 1.5\Omega_e$ is launched from the left boundary. Three vertical dotted lines indicate the position of plasma boundary and where the wave frequency equals the right-handed cutoff frequency, $\omega_{in} = \omega_R$, and upper-hybrid resonance frequency, $\omega_{in} = \omega_{UH}$, respectively.
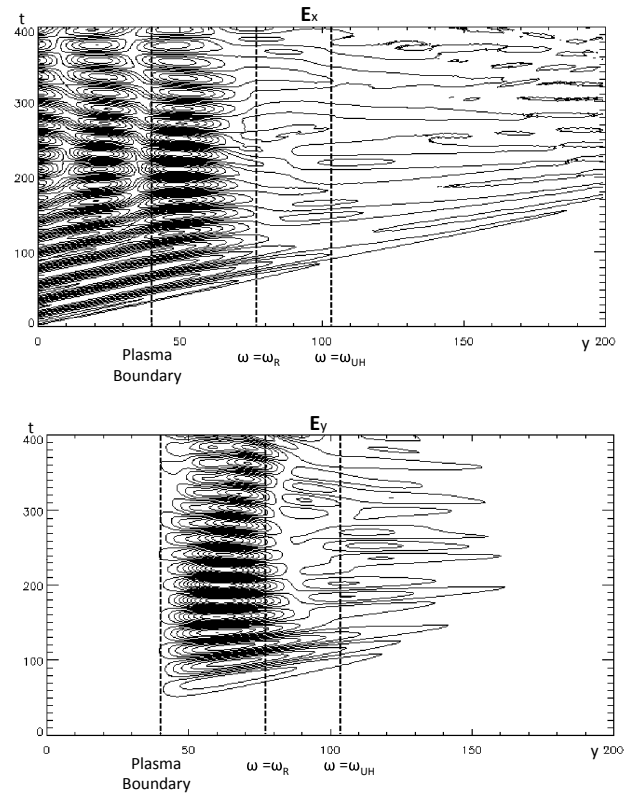
Figure 6: Contour plots depict the volution of E_x and E_y in time and space. The abscissa denotes space coordinate in **y** direction. The ordinate denotes time. Three vertical dotted lines correspond to the characteristic positions in Fig. 5.

The evolution of the electric field perturbation with time and space are displayed in Fig. 6. The behavior of the rf wave in the nonuniform plasma are precisely portrayed. After entering the magnetized plasma, the wave propagates as a fast X wave. The E_y component appears in this region. At the cutoff position, where $\omega_{in}=\omega_R$, the fast X wave is reflected to the left. A portion of the wave energy penetrates the forbidden region for the fast X wave, and continues propagating to the right through the resonance position for the fast X wave, where $\omega_{in}=\omega_{UH}$. On the right of the resonance position, where the fast X waves with original frequency are allowed to propagate, electric field perturbation with complex properties emerge.

To analyse the nonlinear phenomena in this process in detail, we check the spectrum of the high-frequency electric field perturbations at different positions, see Fig. 7 and Fig. 8. It's clearly shown that the waves with the frequency $\omega=2\omega_{in}$ arise at the position y=70. The rf wave doesn't form a steady wave pattern after crossing the resonance region, which reflects the complexity of nonlinear nature of rf physics in the nonuniform magnetized plasmas.
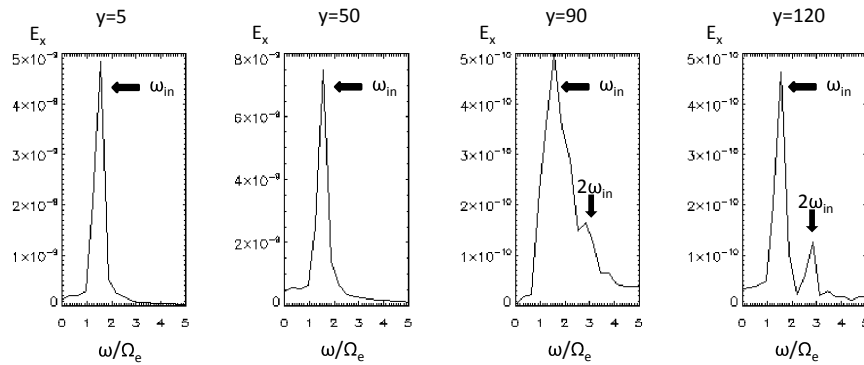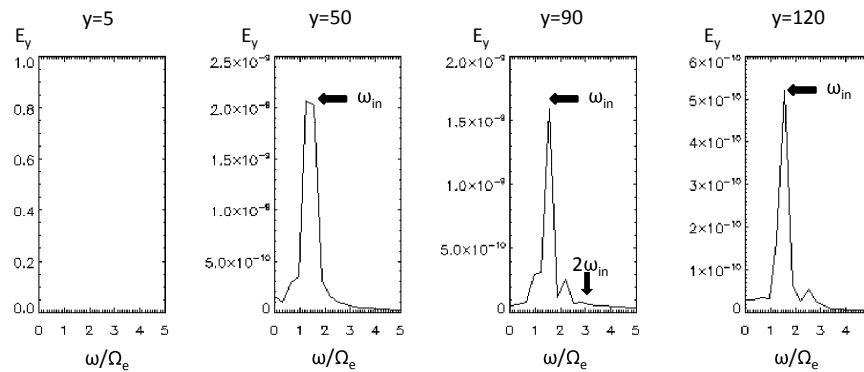
Figure 7: Spectrum of E_x at different positions, $y=5$, $y=50$, $y=90$, and $y=120$ respectively. The abscissa denotes the ratio between frequency and electron gyro-frequency ω/Ω_e. The frequency of injection wave is $\omega_{in}=1.5\Omega_e$.

Figure 8: Spectrum of E_y at different positions, $y=5$, $y=50$, $y=90$, and $y=120$ respectively. The abscissa denotes the ratio between frequency and electron gyro-frequency ω/Ω_e. The frequency of injection wave is $\omega_{in}=1.5\Omega_e$.

4 Discussions

In this paper, the nonlinear PIC algorithm based on gyrocenter gauge kinetic theory for high frequency electromagnetic waves in magnetized plasmas have been developed. The manipulation of particle dynamics, the current density, and the perturbation field have been discussed in detail. To successfully apply this algorithm, the reduction of numerical noises is a technical but important problem. In PIC simulation, the sampling of particles on Lagrangian grids is very coarse because of the limit of now available computational ability [16]. So numerical noises may grow large enough to exceed the physical perturbation fields and lead to the failure of simulations. In δf method, the equilibrium quantities are set fixed and only perturbations are considered. This operation enhances the efficiency of sampling. Instead, we employ another approach to solve the problem of numerical noises in the nonlinear gyrocenter gauge algorithm. Main numerical noise

in the full-f PIC simulation comes from the unperturbed trajectories of particles. In Gy-roGauge code, when calculating current density, the numerical noises from unperturbed trajectories are subtracted directly, because it's easy to obtain the unperturbed trajectories of the sampling particles. Besides, other methods, such as smoothing functions and the sampling optimization, can also be utilized to reduce the numerical noise [17].

The numerical cases in Section 3 have verified the correctness and effectiveness of the nonlinear algorithm based on gyrocenter gauge kinetic theory. Both linear and nonlinear physics can be proper simulated. In the future work, we plan to apply this algorithm to integrated rf wave simulation with real tokamak geometry. The nonlinear gyrocenter gauge kinetic algorithm can be used to explore more high-frequency wave problems in the research of magnetized plasmas.

Acknowledgments

References

[1] N. J. Fisch. Confining a tokamak plasma with rf-driven currents. Phys. Rev. Lett., 41:873–876, 1978.

[2] N. J. Fisch. Theory of current drive in plasmas. Rev. Mod. Phys., 59:175–234, 1987.

[3] V. E. Golant and V. I. Fedorov. RF plasma heating in toroidal fusion devices. Consultants Bureau, New York, 1989.

[4] W. Hooke. Review of experiments on current drive in tokamaks by means of rf waves. Plasma Phys. Contol. Fusion, 26:133, 1984.

[5] X. Y. Guan, H. Qin, J. Liu, and N. J. Fisch. On the toroidal plasma rotations induced by lower hybrid waves. Phys. Plasmas, 20:022502, 2013.

[6] A. Ince-Cushman, J. E. Rice, M. Reinke, M. Greenwald, G. Wallace, R. Parker, C. Fiore, J. W. Hughes, P. Bonoli, S. Shiraiwa, A. Hubbard, S. Wolfe, I. H. Hutchinson, E. Marmar, M. Bitter, J. Wilson, and K. Hill. Observation of self-generated flows in tokamak plasmas with lower-hybrid-driven current. Phys. Rev. Lett., 102:035002, 2009.

[7] J. E. Rice, A. C. Ince-Cushman, P. T. Bonoli, M. J. Greenwald, J. W. Hughes, R. R. Parker, M. L. Reinke, G. M. Wallace, C. L. Fiore, R. S. Granetz, A. E. Hubbard, J. H. Irby, E. S. Marmar, S. Shiraiwa, S. M. Wolfe, S. J. Wukitch, M. Bitter, K. Hill, and J. R. Wilson. Observations of counter-current toroidal rotation in alcator c-mod lhcd plasmas. Nulc. Fusion, 49:025004, 2009.

[8] Z. Yu and H. Qin. Gyrocenter-gauge kinetic algorithm for high frequency waves in magnetized plasmas. Phys. Plasmas, 16:032507, 2009.

[9] H. Qin, R. H. Cohen, W. M. Nevins, and X. Q. Xu. Geometric gyrokinetic theory for edge plasmas. Phys. Plasmas, 14:056110, 2007.

[10] H. Qin and W. M. Tang. Pullback transformations in gyrokinetic theory. Phys. Plasmas, 11:1052, 2004.

[11] H. Qin, W. M. Tang, and W. W. Lee. Gyrocenter-gauge kinetic theory. Phys. Plasmas, 7:4433, 2000.

[12] H. Qin. Topics in kinetic theory. Fields Institute Communications, 46:171–192, 2005.

[13] R. A. Kolesnikov, W.W. Lee, and H. Qin. Electromagnetic high frequency gyrokinetic particle-in-cell simulation. Commun. Comput. Phys., 4:171–192, 2008.

[14] R. A. Kolesnikov, W.W. Lee, H. Qin, and E. Startsev. High frequency gyrokinetic particle simulation. Phys. Plasmas, 14:072506, 2007.

[15] T. D. Stix. Waves in Plasmas. American Institute of Physics, 1992.

[16] A. B. Birdsall and C. K. Langdon. Plasma Physics Via Computer Simulation. Elsevier Science, New York, 1991.

[17] G. R. Liu and M. N. Liu. Smoothed Particle Hydrodynamics a Meshfree Particle Method. World Scientific, 2003.